Hard biaxial ellipsoids revisited: numerical results

Carl McBride and Enrique Lomba

Instituto de Química Física Rocasolano (CSIC), Serrano 119, 28006 Madrid, Spain

(Dated: November 14, 2006)

Monte Carlo simulations are performed for hard ellipsoids for a number of values of its semi-axes in the range $c/a \in \{0.1, 10\}$. The isotropic phase results are compared to the Vega equation of state [Mol. Phys. **92** 651 (1997)]. The position of the isotropic-nematic transition is also evaluated. The biaxial phase is seen to form only after the previous formation of a discotic phase.

INTRODUCTION

One of the first ever models used in computer simulation studies of the fluid phase was the hard sphere. The next most obvious choice of model is the hard ellipsoid; an affine transformation of the hard sphere. The orientation of the model now becomes a variable within the simulation. Having a model that incorporates orientation facilitates the study of orientationally ordered phases, such as those associated with liquid crystals.

As with hard spheres [1, 2, 3, 4] the first simulations of hard ellipsoids were performed for two-dimensional systems [5, 6]. Hard spheres are only capable of forming two phases; the fluid and the solid. There is no 'gas-liquid' transition, due to the lack of attractive forces. However, the hard ellipsoid system also has a plastic crystal (for small axis ratios) and a nematic phase. Prolate and prolate-like biaxial models, *i.e.* models of the form $a \leq b < c$ with $b < \sqrt{ac}$ where a, b and c are the semi-axes of the ellipsoid, are able to form a uniaxial nematic phase, often denominated as N_+. Oblate and oblate-like biaxial models, with $a < b \leq c$ and $b > \sqrt{ac}$, can form a uniaxial 'discotic' phase (N_-). A tentative phase diagram for uniaxial ellipsoids was proposed by Frenkel and co-workers [7, 8, 9, 10]. As well as these nematic and discotic phases, Freiser [11] predicted that 'long-flat' molecules could form a biaxial phase N_B, which has recently been discovered experimentally [12, 13].

The study of hard bodies provide reference systems for use in perturbation theories which add long range attractive interactions [14]. They can also form the monomer units of larger molecules [15, 16]. Hard ellipsoids continue to be of interest [17, 18], having recently been shown that a maximally random jammed (MRJ) packing fraction of $\phi = 0.7707$ is possible for models whose maximal aspect ratio is greater than $\sqrt{3}$. [19, 20], Such high packing fractions were obtained using an 'event-driven' molecular dynamics code [21, 22] and were confirmed experimentally using latex particles and the like [23, 24].

Biaxial ellipsoids have, however, received comparatively little attention, simulations having been performed principally by Allen [25] and by Camp and Allen [26]. Extensive simulation results have been presented previously for uniaxial hard ellipsoids, notably those of Frenkel and Mulder for c/a in the range [1/3, 3] [9] In this publication a number of simulations are performed for biaxial ellipsoids within the region c/a for [0.1, 10]. Also in this work the isotropic equation of state is compared to theory.

SIMULATION TECHNIQUE

Standard Metropolis Monte Carlo sampling was used [1]. The decision to reject or accept a trial move for hard bodies is based simply on whether two bodies overlap or not. For hard spheres ($a = b = c$) this criteria is trivial; if the distance between two bodies is less than twice the radius then they overlap. For hard ellipsoids the situation is more complicated, having to take into account the orientations of the ellipsoids as well as the distance between them. One of the first overlap criteria was proposed for two-dimensional ellipsoids by Vieillard-Baron [5, 27]. Perram and Wertheim produced an overlap algorithm for three-dimensional ellipsoids [28]. In this study the Perram-Wertheim criteria was used.

All of the Monte Carlo simulations were performed in the NpT ensemble (with $k_BT = 1$), having cubic boundary conditions, with the system comprising of $N = 343$ hard ellipsoids. The runs consisted of between 75 and 150 kilocycles for equilibration followed by a further 75-150 kilocycles for the production of thermodynamic data. Each simulation was initiated from the final configuration of the previous, lower pressure, run. Throughout the simulations the uniaxial order parameter S_2 was monitored for each of the three axis by calculating

$$S_2 = \left\langle \frac{1}{2}(3\cos^2\theta_i - 1) \right\rangle, \tag{1}$$

where θ_i is the angle between ellipsoid i and the director vector [29, 30, 31].

The prolate parameters are typified by $a = b$, the oblate parameters by $b = c$ and the biaxial parameters by $a \neq b \neq c$ where in this work $a < b < c$ (in this work we define $a = 1$).

Boublik and Nezbeda have shown [32] that hard convex bodies can be described using three geometric expressions; the volume, V, the surface area, S and the mean radius of curvature, R. The second virial coefficient, B_2 for any hard convex body is given by the Isihara-Hadwiger formula [33, 34], and provides a measure of the excluded

volume of a 'molecule' due to the presence of a second molecule,

$$B_2 = RS + V, \qquad (2)$$

or

$$\frac{B_2}{V} = 1 + 3\alpha, \qquad (3)$$

if one defines the 'non-sphericity' parameter [35]

$$\alpha = \frac{RS}{3V}. \qquad (4)$$

Values for R, S and V for ellipsoids are provided in Appendix A.

RESULTS

Isotropic phase equation of state

Accurate equations of state (EOS) are necessary if the hard ellipsoid fluid is to be used as a reference system in perturbation theories. A number of equations of state have been proposed over the years to reproduce the behaviour of the isotropic phase of the ellipsoid system; notably those of Nezbeda [36], Parsons [37], and Song and Mason [38]. It should be noted that all of these equations of state implicitly assume that the EOS is symmetric with respect to prolate/oblate models, since they are built either directly using B_2, or indirectly using α. This is because $B_2(1 \times 1 \times x) = B_2(1 \times x \times x)$.

In order to reproduce simulation results, higher virial coefficients are required, where it has been shown that the prolate/oblate symmetry breaks down starting from B_3 [39, 40], as used in the uniaxial EOS of Maeso and Solana [41] or the biaxial EOS of Vega [42]. In this work the simulation results are compared to the biaxial Vega equation of state. The Vega EOS is given by

$$
\begin{aligned}
Z = \ & 1 \ + B_2^* y + B_3^* y^2 + B_4^* y^3 + B_5^* y^4 \\
& + \frac{B_2}{4} \left(\frac{1 + y + y^2 - y^3}{(1-y)^3} \right. \\
& \left. - 1 - 4y - 10y^2 - 18.3648y^3 - 28.2245y^4 \right), \quad (5)
\end{aligned}
$$

where Z is the compressibility factor and y is the volume fraction, given by $y = \rho V$ where ρ is the number density. The virial coefficients are given by the fits

$$
\begin{aligned}
B_3^* = \ & 10 + 13.094756\alpha' - 2.073909\tau' + 4.096689\alpha'^2 \\
& + 2.325342\tau'^2 - 5.791266\alpha'\tau', \qquad (6)
\end{aligned}
$$

$$
\begin{aligned}
B_4^* = \ & 18.3648 + 27.714434\alpha' - 10.2046\tau' + 11.142963\alpha'^2 \\
& + 8.634491\tau'^2 - 28.279451\alpha'\tau' \\
& - 17.190946\alpha'^2\tau' + 24.188979\alpha'\tau'^2 \\
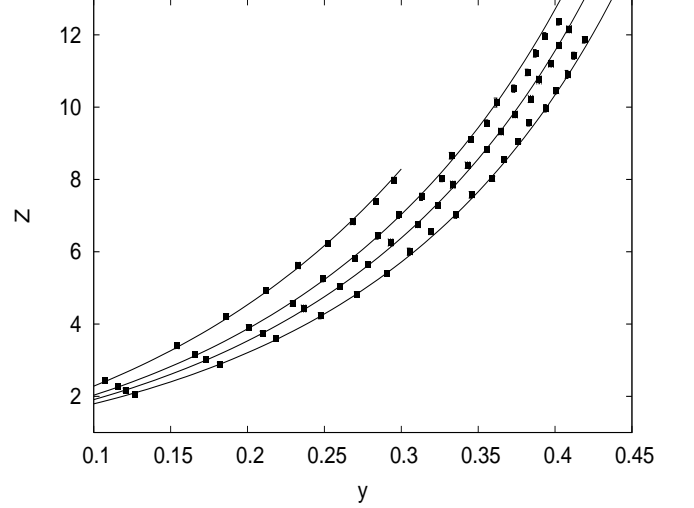& + 0.74674\alpha'^3 - 9.455150\tau'^3, \qquad (7)
\end{aligned}
$$

FIG. 1: Plot of the simulation results for the biaxial molecules $1 \times 2 \times 4$, $1 \times 2 \times 5$, $1 \times 2 \times 6$ and the isotropic state points for $1 \times 2 \times 8$. The lines are the Vega equation of state.

and

$$
\begin{aligned}
B_5^* = \ & 28.2245 + 21.288105\alpha' + 4.525788\tau' + 36.032793\alpha'^2 \\
& + 59.0098\tau'^2 - 118.407497\alpha'\tau' \\
& + 24.164622\alpha'^2\tau' + 139.766174\alpha'\tau'^2 \\
& - 50.490244\alpha'^3 - 120.995139\tau'^3 + 12.624655\alpha'^3\tau', \quad (8)
\end{aligned}
$$

where

$$\tau' = \frac{4\pi R^2}{S} - 1, \qquad (9)$$

and

$$\alpha' = \frac{RS}{3V} - 1. \qquad (10)$$

Values for R and S for the models studied in the work are given in Appendix A.

The effect of varying c for a biaxial model is shown in Fig. 1, where various models from Table I are plotted. As can be seen, the Vega EOS provides an excellent fit for all of the isotropic state points. This is also demonstrated in a plot of the self-dual models, where $b = \sqrt{ac}$ (Fig. 2) taken from Table II. In figures 3 and 4 the isotropic equations of state are plotted for the $1 \times 2.5 \times 2.5$, $1 \times 1 \times 2.5$ and for the $1 \times 4 \times 4$, and $1 \times 1 \times 4$ models. It can be seen that for these modest anisotropies the oblate/prolate curves are indeed almost coincident, as assumed in the simple EOS built using B_2 only. The numerical results are presented in Tables III and IV.

Isotropic-liquid crystal transition

The theory behind the isotropic-nematic (I-N) transition was first developed by Lars Onsager [43] and was

TABLE I: Equations of state for biaxial ($a = 1$, $a < b < c$) hard ellipsoids. Error in y is $O(10^{-3})$, error in Z is $O(10^{-2}$)

| p^*	$b=2,c=5$		$b=2,c=6$		$b=2,c=8$		$b=3,c=6$		$b=3,c=8$		$b=3,c=10$		$b=5,c=8$		$b=5,c=10$		$b=8,c=10$	
	y	Z	y	Z	y	Z	y	Z	y	Z	y	Z	y	Z	y	Z	y	Z
0.5	0.120	2.17	0.115	2.26	0.107	2.43	0.114	2.28	0.107	2.44	0.102	2.56	0.103	2.52	0.097	2.67	0.093	2.80
1.0	0.173	3.02	0.166	3.15	0.154	3.39	0.165	3.16	0.153	3.40	0.145	3.60	0.146	3.56	0.141	3.70	0.134	3.89
1.5	0.209	3.74	0.200	3.91	0.186	4.21	0.198	3.96	0.196	4.21	0.176	4.45	0.180	4.34	0.170	4.59	0.165	4.74
2.0	0.236	4.42	0.229	4.56	0.211	4.94	0.227	4.60	0.212	4.93	0.200	5.21	0.206	5.06	0.199	5.25	0.194	5.39
2.5	0.259	5.03	0.249	5.25	0.232	5.62	0.246	5.30	0.233	5.60	0.224	5.82	0.226	5.77	0.220	5.93	0.219	5.96
3.0	0.278	5.64	0.270	5.81	0.252	6.22	0.269	5.82	0.253	6.20	0.243	6.45	0.249	6.30	0.243	6.44	0.249	6.29
3.5	0.293	6.25	0.284	6.43	0.268	6.83	0.283	6.45	0.272	6.72	0.258	7.08	0.270	6.76	0.269	6.80	0.286	6.40
4.0	0.310	6.74	0.298	7.01	0.283	7.38	0.297	7.03	0.284	7.36	0.280	7.48	0.288	7.25	0.301	6.95	0.308	6.78
4.5	0.323	7.27	0.313	7.51	0.295	7.97	0.310	7.59	0.302	7.77	0.292	8.05	0.313	7.51	0.320	7.34	0.327	7.19
5.0	0.333	7.85	0.326	8.01	0.310	8.43	0.324	8.06	0.314	8.33	0.310	8.43	0.338	7.73	0.334	7.83	0.341	7.67
5.5	0.343	8.39	0.332	8.65	0.323	8.90	0.333	8.63	0.330	8.70	0.328	8.77	0.352	8.17	0.349	8.23	0.357	8.05
6.0	0.355	8.82	0.345	9.09	0.342	9.16	0.345	9.09	0.338	9.28	0.345	9.08	0.363	8.63	0.361	8.68	0.365	8.58
6.5	0.364	9.32	0.356	9.56	0.357	9.52	0.355	9.58	0.363	9.37	0.355	9.58	0.372	9.13	0.371	9.17	0.377	9.01
7.0	0.374	9.79	0.361	10.12	0.370	9.88	0.362	10.11	0.367	9.98	0.366	9.99	0.388	9.43	0.381	9.60	0.391	9.36
7.5	0.384	10.22	0.373	10.51	0.390	10.05	0.370	10.60	0.379	10.33	0.378	10.37	0.397	9.88	0.391	10.04	0.398	9.84
8.0	0.389	10.75	0.382	10.96	0.395	10.59	0.385	10.87	0.387	10.80	0.389	10.76	0.410	10.20	0.399	10.48	0.409	10.24
8.5	0.397	11.19	0.387	11.48	0.399	11.13	0.394	11.27	0.399	11.13	0.392	11.33	0.414	10.72	0.411	10.81	0.419	10.62
9.0	0.402	11.70	0.393	11.96	0.415	11.35	0.402	11.70	0.406	11.59	0.395	11.90	0.421	11.17	0.415	11.34	0.425	11.06
9.5	0.409	12.15	0.402	12.35	0.421	11.78	0.409	12.15	0.414	12.00	0.408	12.17	0.432	11.49	0.420	11.82	0.432	11.50
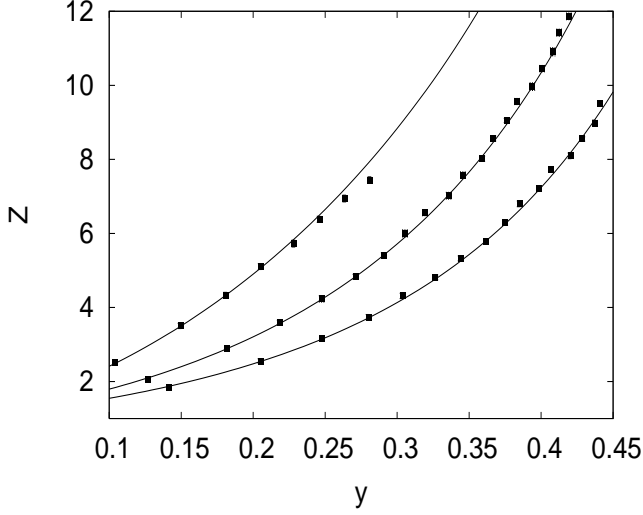
FIG. 2: Plot of the simulation results for the self-dual molecules $1 \times 1.25 \times 1.5625$, $1 \times 2 \times 4$ and the isotropic state points for $1 \times 3 \times 9$. The lines are the Vega equation of state.
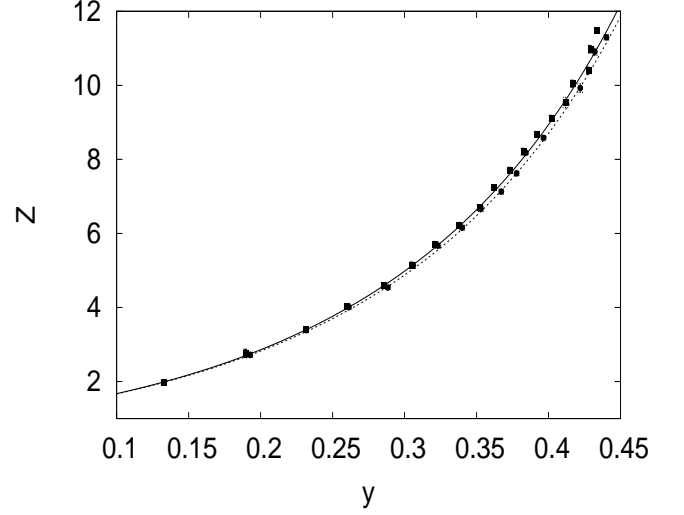

FIG. 3: Plot of the results for the oblate $1 \times 2.5 \times 2.5$ model (black squares) and the prolate $1 \times 1 \times 2.5$ model (black circles) along with the Vega EOS (oblate: solid line, prolate: dashed line)

TABLE II: Equations of state for biaxial self-dual ($b = \sqrt{ac}$) hard ellipsoids. Error in y is $O(10^{-3})$, error in Z is $O(10^{-2})$

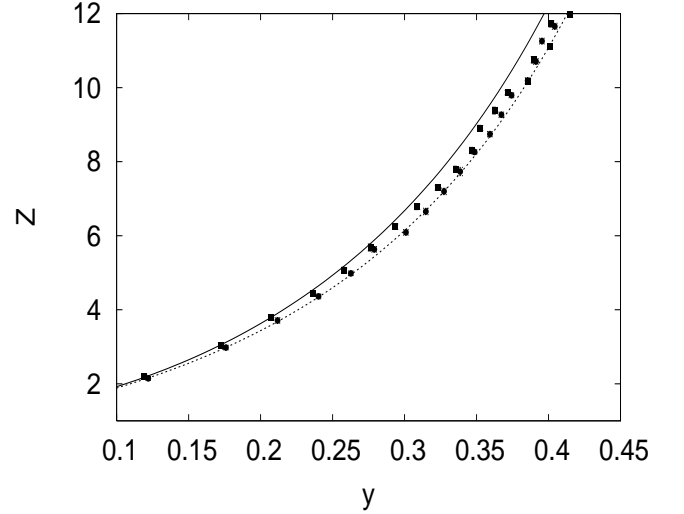|	$b = 1.25, c = 1.5625$		$b = 2, c = 4$		$b = 3, c = 9$	
p^*	y	Z	y	Z	y	Z
0.5	0.141	1.85	0.126	2.06	0.104	2.51
1.0	0.205	2.55	0.181	2.87	0.149	3.50
1.5	0.247	3.17	0.218	3.59	0.181	4.33
2.0	0.280	3.73	0.247	4.23	0.205	5.10
2.5	0.303	4.31	0.271	4.82	0.228	5.76
3.0	0.326	4.81	0.290	5.40	0.246	6.38
3.5	0.344	5.32	0.305	6.00	0.264	6.94
4.0	0.361	5.79	0.319	6.55	0.281	7.44
4.5	0.375	6.28	0.335	7.01	0.301	7.82
5.0	0.385	6.79	0.345	7.57	0.315	8.29
5.5	0.389	7.22	0.359	8.01	0.332	8.67
6.0	0.406	7.72	0.366	8.56	0.344	9.12
6.5	0.420	8.09	0.376	9.04	0.356	9.54
7.0	0.428	8.55	0.383	9.56	0.364	10.06
7.5	0.437	8.97	0.394	9.96	0.376	10.41
8.0	0.441	9.49	0.400	10.45	0.384	10.88
8.5	0.451	9.86	0.408	10.90	0.395	11.26
9.0	0.458	10.28	0.412	11.42	0.406	11.58
9.5	0.463	10.72	0.419	11.86	0.410	12.11

FIG. 4: Plot of the results for the oblate $1 \times 4 \times 4$ model (black squares) and the prolate $1 \times 1 \times 4$ model (black circles) along with the Vega EOS (oblate: solid line, prolate: dashed line)

studied for solutions of hard ellipsoids by Akira Isihara [44]. Frenkel and Mulder [9, 10] found an I-N$_+$ transition for a system of $\approx 90-108$ prolate ellipsoids of $c/a \geq 2.75$. This result was called into question by Zarragoicoechea *et al.* [45], suggesting system size effects play an important role in locating the I-N transition. However, a later work by Allen and Mason [46] confirmed the nematic phase for

$c/a = 3.0$ at densities of $\rho/\rho_{cp} \approx 0.73-0.75$. In this work no such transition is found until $c/a = 6$. It is interesting to compare this to linear tangent hard spheres, where nematic phases were found for $m = 6$ and a smectic A phase for $m = 5$ where m is the number of monomer units [47] (Note that smectic phases are not observed for hard ellipsoids).

The appearance of the nematic phase for the $1 \times 1 \times 8$ (Fig. 7) model was considerably 'delayed', and no nematic phase formed for compression runs (150k equilibration followed by 150k production) of the prolate $1 \times 1 \times 10$

TABLE III: Equations of state for oblate ($a = 1$, $b = c$) hard ellipsoids. Error in y is $O(10^{-3})$, error in Z is $O(10^{-2})$

	c	2.5		4		5		6		8		10
p^*	y	Z	y	Z	y	Z	y	Z	y	Z	y	Z
0.5	0.132	1.97	0.119	2.19	0.113	2.31	0.108	2.41	0.097	2.70	0.090	2.90
1.0	0.189	2.76	0.172	3.03	0.162	3.23	0.153	3.40	0.140	3.71	0.129	4.03
1.5	0.231	3.39	0.207	3.78	0.196	4.00	0.185	4.24	0.171	4.57	0.161	4.85
2.0	0.260	4.02	0.236	4.43	0.220	4.75	0.213	4.91	0.195	5.34	0.192	5.45
2.5	0.285	4.58	0.258	5.07	0.243	5.38	0.233	5.61	0.226	5.76	0.240	5.44
3.0	0.305	5.14	0.276	5.68	0.263	5.96	0.252	6.21	0.257	6.10	0.270	5.80
3.5	0.321	5.70	0.293	6.24	0.282	6.49	0.273	6.69	0.281	6.51	0.293	6.24
4.0	0.337	6.20	0.308	6.77	0.293	7.13	0.292	7.15	0.307	6.82	0.310	6.73
4.5	0.352	6.69	0.323	7.29	0.312	7.52	0.306	7.69	0.324	7.26	0.326	7.22
5.0	0.362	7.23	0.335	7.79	0.325	8.05	0.327	8.00	0.341	7.65	0.345	7.57
5.5	0.373	7.71	0.346	8.30	0.335	8.58	0.336	8.56	0.351	8.19	0.356	8.08
6.0	0.382	8.21	0.352	8.90	0.348	9.01	0.355	8.82	0.369	8.50	0.371	8.46
6.5	0.391	8.68	0.362	9.38	0.358	9.49	0.375	9.07	0.374	9.09	0.379	8.96
7.0	0.402	9.11	0.371	9.86	0.374	9.78	0.383	9.54	0.394	9.27	0.389	9.42
7.5	0.412	9.52	0.385	10.17	0.386	10.16	0.394	9.95	0.404	9.70	0.399	9.83
8.0	0.417	10.04	0.389	10.75	0.398	10.49	0.404	10.34	0.413	10.13	0.404	10.34
8.5	0.427	10.40	0.400	11.09	0.415	10.72	0.415	10.70	0.416	10.68	0.415	10.72
9.0	0.429	10.97	0.402	11.72	0.422	11.14	0.424	11.09	0.423	11.12	0.421	11.18
9.5	0.433	11.47	0.415	11.98	0.437	11.36	0.431	11.53	0.428	11.60	0.430	11.56

TABLE IV: Equations of state for prolate ($a = b = 1$) hard ellipsoids. Error in y is $O(10^{-3})$, error in Z is $O(10^{-2})$

|	c	2.5		4		5		6		8		10
p^*	y	Z	y	Z	y	Z	y	Z	y	Z	y	Z
0.5	0.132	1.97	0.121	2.14	0.115	2.26	0.110	2.37	0.101	2.56	0.095	2.75
1.0	0.192	2.71	0.175	2.97	0.166	3.14	0.158	3.29	0.145	3.59	0.136	3.84
1.5	0.231	3.38	0.211	3.70	0.200	3.92	0.191	4.09	0.178	4.41	0.166	4.71
2.0	0.261	4.00	0.240	4.36	0.226	4.61	0.218	4.80	0.201	5.19	0.192	5.43
2.5	0.288	4.53	0.262	4.98	0.250	5.22	0.238	5.48	0.222	5.88	0.215	6.06
3.0	0.305	5.13	0.278	5.63	0.268	5.86	0.256	6.13	0.240	6.54	0.228	6.88
3.5	0.323	5.67	0.300	6.09	0.282	6.48	0.277	6.59	0.255	7.17	0.243	7.53
4.0	0.340	6.15	0.314	6.65	0.300	6.96	0.289	7.23	0.269	7.78	0.258	8.11
4.5	0.353	6.66	0.327	7.19	0.314	7.49	0.304	7.74	0.285	8.25	0.269	8.74
5.0	0.367	7.12	0.338	7.73	0.325	8.03	0.311	8.40	0.298	8.77	0.285	9.15
5.5	0.377	7.62	0.348	8.26	0.332	8.67	0.326	8.82	0.311	9.24	0.297	9.68
6.0	0.384	8.17	0.359	8.74	0.346	9.06	0.334	9.39	0.321	9.76	0.308	10.19
6.5	0.396	8.58	0.367	9.26	0.352	9.66	0.349	9.72	0.330	10.30	0.317	10.71
7.0	0.402	9.10	0.374	9.79	0.365	10.03	0.356	10.27	0.349	10.49	0.327	11.17
7.5	0.411	9.53	0.385	10.18	0.373	10.50	0.377	10.40	0.356	11.02	0.334	11.75
8.0	0.422	9.92	0.391	10.70	0.375	11.16	0.389	10.76	0.367	11.40	0.337	12.40
8.5	0.428	10.39	0.395	11.25	0.388	11.46	0.402	11.06	0.376	11.83	0.345	12.86
9.0	0.432	10.90	0.404	11.65	0.394	11.94	0.407	11.55	0.385	12.21	0.356	13.20
9.5	0.440	11.29	0.413	12.01	0.403	12.32	0.417	11.90	0.389	12.75	0.367	13.54
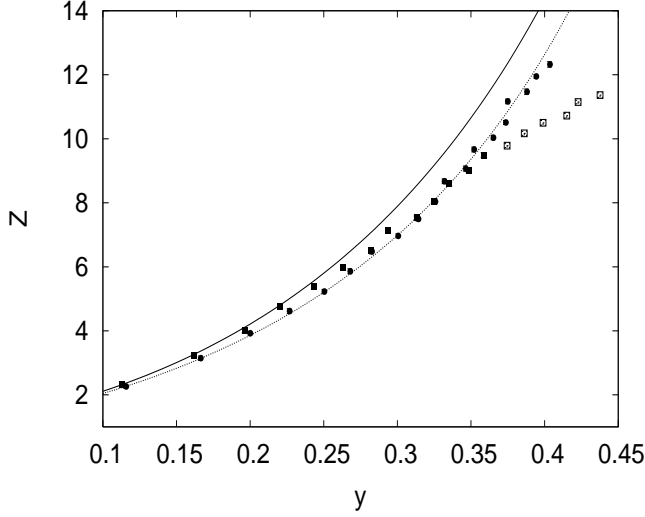
FIG. 5: Plot of the results for the oblate $1 \times 5 \times 5$ model (isotropic: black squares, discotic: open squares) and the prolate $1 \times 1 \times 5$ model (black circles) along with the Vega EOS (oblate: solid line, prolate: dashed line)
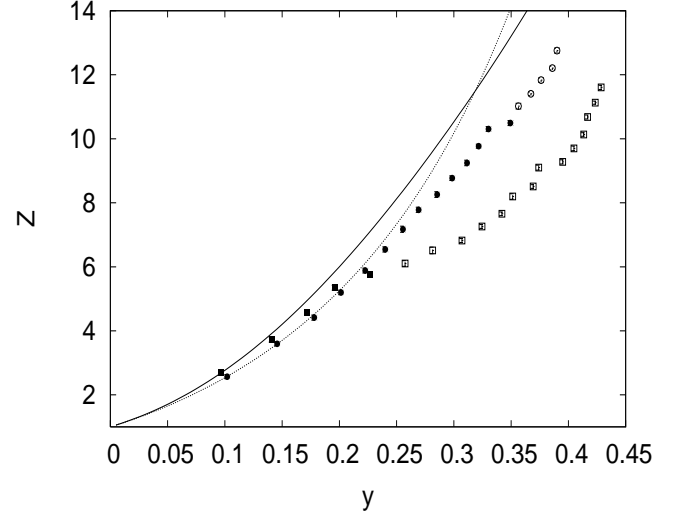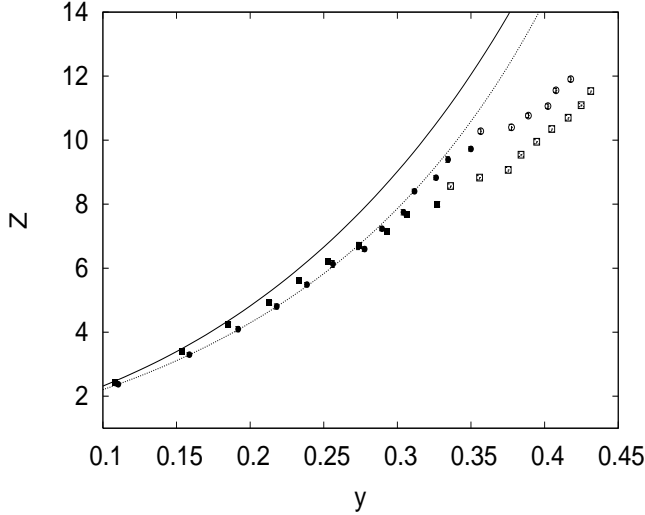

FIG. 7: Plot of isotropic the results for the oblate $1 \times 8 \times 8$ model (isotropic: black squares, discotic: open squares) and the prolate $1 \times 1 \times 8$ model (isotropic: black circles, nematic: open circles) along with the Vega EOS (oblate: solid line, prolate: dashed line)

FIG. 6: Plot of isotropic the results for the oblate $1 \times 6 \times 6$ model (isotropic: black squares, discotic: open squares) and the prolate $1 \times 1 \times 6$ model (isotropic: black circles, nematic: open circles) along with the Vega EOS (oblate: solid line, prolate: dashed line)
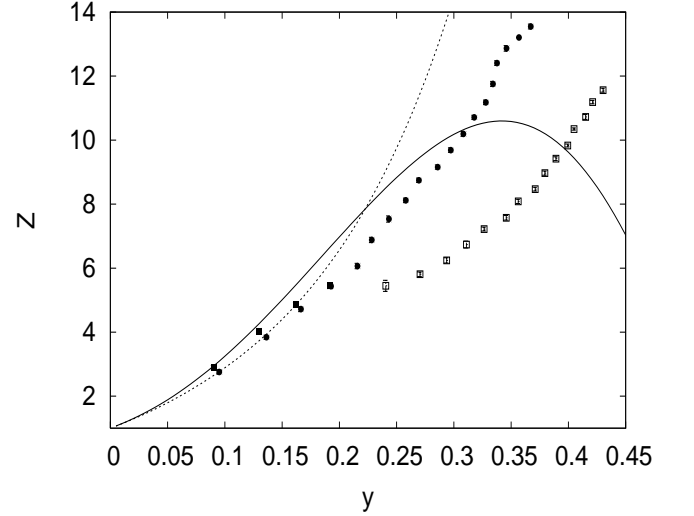

FIG. 8: Plot of the isotropic results for the oblate $1 \times 10 \times 10$ model (isotropic: black squares, discotic: open squares) and the prolate $1 \times 1 \times 10$ model (black circles) along with the Vega EOS (oblate: solid line, prolate: dashed line)

model (Fig. 8). Given that it is fully expected to see N_+ phases for this model this indicates that so called 'jamming' is a real problem for especially elongated prolate systems. The system finds itself grid-locked, and is unable to reorientate into the energetically more favourable nematic phase within the time scale of the simulation. The equation of state of the glassy state (Fig. 8) can be seen to be intermediate between the higher compressibility factor of the isotropic phase, indicated by the Vega

EOS, and the much lower values for the discotic branch of the $1 \times 10 \times 10$ model. On the other hand, discotic phases readily appeared for the $1 \times 5 \times 5$ model (Fig. 5) upwards.

Samborski *et al.* [48] placed the I-N transition at $0.370 < y < 0.388$ for the $1 \times 1 \times 5$ model, $0.333 < y < 0.351$ for the $1 \times 5 \times 5$ model, $0.203 < y < 0.222$ for the $1 \times 1 \times 10$ model and $0.185 < y < 0.203$ for the $1 \times 10 \times 10$ model. It is interesting to note that I-N transi-
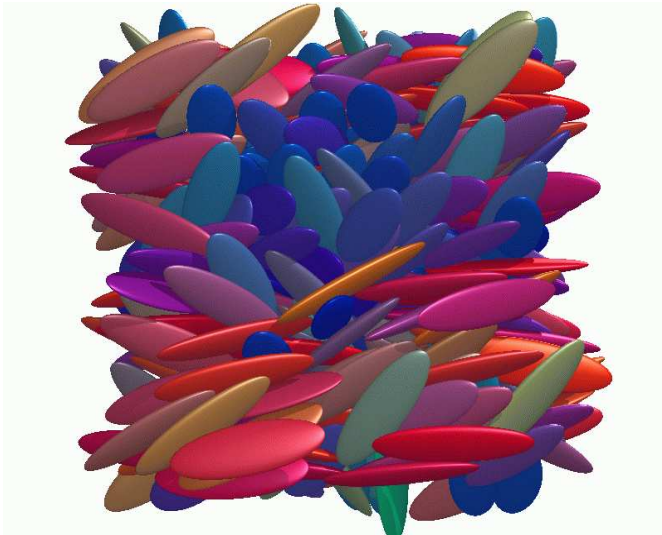
FIG. 9: Snap-shot of the $1 \times 3 \times 10$ model in the biaxial phase (here at $p^* = 8.0$). The ellipsoids are colour coded with respect to their orientations (colour online).
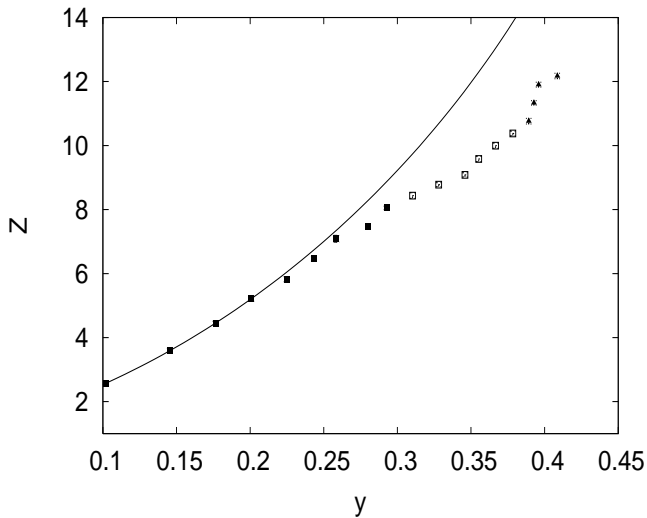

FIG. 10: Plot of the equation of state for the biaxial $1 \times 3 \times 10$ model (isotropic: black squares, discotic: open squares, biaxial: black triangles) along with the Vega EOS for the isotropic branch.

tion sets in at lower volume fractions for oblate ellipsoids than for prolate models that have the same value of c. The same is seen in this work for the '6' (Fig. 6) and '8' (Fig. 7) models. This is probably due to the fact that the compressibility factor of the oblate models, for a given volume fraction, is higher than that of its corresponding prolate counterpart. This triggers the earlier onset of the I-N$_-$ transition.

In this study only one convincing biaxial phase was identified, that of the $1 \times 3 \times 10$ model (see Fig. 9 for a snapshot, Fig. 10 for the EOS). The biaxial phase

formed at $p^* = 8.0$, however, at $p^* = 5.0$ the system had formed a discotic phase. This indicates that the formation of a biaxial phase is a two-stage process; first orientating along the short a axis, later followed by the long c axis *i.e.* having the phase transitions isotropic - discotic - biaxial. This is in line with the observation that discotic phases form at lower volume fractions than nematic phases (the biaxial phase can be seen as being composed of both a discotic and a nematic phase).

The positions of the isotropic liquid-liquid crystal transitions found in this work are presented in Table V. A study of the I-N transition for biaxial ellipsoids was undertaken by Tjipto-Margo and Evans [49] confirming the finding of Gelbart and Barboy [50] that biaxiality reduces the first order nature of the I-N transition (this result was also confirmed for hard sphero-platelets by Somoza and Tarazona [51]). It appears that the additional degree of freedom associated with biaxiality increases the disorder in the nematic phase with respect to a uniaxial ($D_{\infty h}$) model. At the 'self-dual' point (where $a : b = b : c$, i.e. $b = \sqrt{ac}$) the transition becomes second-order [52]. The isotropic-biaxial nematic transition is said to occur for models that are close to this self-dual point [25]. For the uniaxial $1 \times 10 \times 10$ model a considerable jump can be seen in the volume fractions associated with the formation of the discotic phase (Fig. 8), one of the hall-marks of a first-order transition. Meanwhile, for the biaxial $1 \times 3 \times 10$ model no such jump is seen.

CONCLUSIONS

Various ellipsoidal models have been subjected to Monte Carlo compression runs. The Vega equation of state is seen to perform very well for the isotropic phases of all of the models considered. The elongated uniaxial models show indications of the first-order nature of the isotropic-nematic transition. However, the formation of orientationally ordered phases for very long prolate models is severely hindered by the formation of a glass like state. The oblate models form discotic readily, at lower volume fractions than their prolate partners. The biaxial phase seems to form in a two-stage process, first forming a discotic phase, followed by the biaxial phase upon orientation of the long axes.

TABLE V: Location of the isotropic-nematic transition ($S_2 > 0.4$) for hard ellipsoids (Note: $a = 1$). Order parameters are given for $p^* = 9.5$.

b	c	p^*	y	phase	$S_2(c)$	$S_2(a)$
prolate						
1	2.5	–	–	I	< 0.1	< 0.1
1	4	–	–	I	< 0.1	< 0.1
1	5	–	–	I	0.13	< 0.1
1	6	7.0	0.356	N_+	0.69	0.20
1	8	7.5	0.356	N_+	0.55	0.18
1	10	–	–	I	0.30	0.12
oblate						
2.5	2.5	–	–	I	< 0.1	< 0.1
4	4	–	–	I	0.12	0.24
5	5	7.0	0.374	N_-	0.23	0.81
6	6	5.5	0.336	N_-	0.25	0.87
8	8	3.0	0.257	N_-	0.26	0.92
10	10	2.5	0.240	N_-	0.27	0.95
biaxial prolate	$(b < \sqrt{ac})$					
2	5	–	–	I	0.10	< 0.1
2	6	–	–	I	0.21	0.15
2	8	6.0	0.342	N_+	0.85	0.25
3	10	8.0	0.389	B	0.48	0.76
biaxial self-dual						
1.25	1.5625	–	–	I	< 0.1	< 0.1
2	4	–	–	I	< 0.1	< 0.1
3	9	4.5	0.30	N_-	0.34	0.81
biaxial oblate	$(b > \sqrt{ac})$					
3	6	9.0	0.402	N_-	0.23	0.46
3	8	6.0	0.338	N_-	0.27	0.78
5	8	4.5	0.313	N_-	0.25	0.90
5	10	3.5	0.269	N_-	0.30	0.92
8	10	3.0	0.249	N_-	0.27	0.95

TABLE VI: Values for R, S, V, α and B_2/V for hard ellipsoids (Note: $a = 1$).

b	c	R	S	V	α	B_2/V
sphere						
1	1	1	4π	$4\pi/3$	1	4
prolate						
1	2.5	1.5919	26.1518	10.472	1.32516	4.97549
1	4	2.26639	40.4975	$16\pi/3$	1.82597	6.4779
1	5	2.73397	50.1925	$20\pi/3$	2.184	7.552
1	6	3.20942	59.9386	8π	2.55136	8.65409
1	8	4.17441	79.5147	$32\pi/3$	3.30174	10.9052
1	10	5.15042	99.151	$40\pi/3$	4.06377	13.1913
oblate						
2.5	2.5	2.0811	50.0111	26.1799	1.32516	4.97549
4	4	3.22269	113.921	$64\pi/3$	1.82597	6.4779
5	5	3.99419	171.78	$100\pi/3$	2.184	7.552
6	6	4.76976	241.985	48π	2.55136	8.65409
8	8	6.32758	419.657	$256\pi/3$	3.30174	10.9052
10	10	7.89019	647.22	$400\pi/3$	4.06377	13.1913
biaxial						
1.25	1.5625	1.28328	20.1576	8.18123	1.05395	4.16185
2	4	2.52566	63.4766	$32\pi/3$	1.59473	5.7842
2	5	2.96925	78.2743	$40\pi/3$	1.84951	6.54853
2	6	3.42527	93.1895	16π	2.11675	7.35026
2	8	4.36059	123.218	$64\pi/3$	2.67234	9.01701
3	6	3.70789	129.13	24π	2.11675	7.35026
3	8	4.60996	170.448	32π	2.60536	8.81607
3	9	5.07182	191.203	36π	2.85815	9.57446
3	10	5.53883	212.0	40π	3.11474	10.3442
5	8	5.22725	268.73	$160\pi/3$	2.7946	9.38379
5	10	6.10332	333.946	$200\pi/3$	3.24386	10.7316
8	10	7.1304	521.211	$320\pi/3$	3.69682	12.0904

APPENDIX A

In Table VI we provide a table of R, S, V, α and B_2/V for the various models studied in this work. The values for R and S are obtained by evaluating the expressions derived by Singh and Kumar [53, 54]. Thus the mean radius of curvature is given by

$$R = \frac{a}{2}\left[\sqrt{\frac{1+\epsilon_b}{1+\epsilon_c}} + \sqrt{\epsilon_c}\left\{\frac{1}{\epsilon_c}F(\varphi, k_1) + E(\varphi, k_1)\right\}\right], \tag{11}$$

and the surface area by

$$S = 2\pi a^2\left[1 + \sqrt{\epsilon_c(1+\epsilon_b)}\left\{\frac{1}{\epsilon_c}F(\varphi, k_2) + E(\varphi, k_2)\right\}\right], \tag{12}$$

where $F(\varphi, k)$ is an elliptic integral of the first kind and $E(\varphi, k)$ is an elliptic integral of the second kind, with the amplitude being

$$\varphi = \tan^{-1}(\sqrt{\epsilon_c}), \tag{13}$$

and the moduli

$$k_1 = \sqrt{\frac{\epsilon_c - \epsilon_b}{\epsilon_c}}, \tag{14}$$

and

$$k_2 = \sqrt{\frac{\epsilon_b(1+\epsilon_c)}{\epsilon_c(1+\epsilon_b)}}, \tag{15}$$

where the anisotropy parameters, ϵ_b and ϵ_c, are

$$\epsilon_b = \left(\frac{b}{a}\right)^2 - 1, \tag{16}$$

and

$$\epsilon_c = \left(\frac{c}{a}\right)^2 - 1. \tag{17}$$

The volume of the ellipsoid is given by the well known

$$V = \frac{4\pi}{3} abc. \tag{18}$$

Note the symmetry between the prolate and oblate ellipsoids for the values of α, and thus for B_2.

---

[1] N. Metropolis, A. W. Rosenbluth, M. N. Rosenbluth, A. H. Teller, and E. Teller, J. Chem. Phys. **21**, 1087 (1953).
[2] B. J. Alder and T. E. Wainwright, J. Chem. Phys. **27**, 1208 (1957).
[3] W. W. Wood, Los Alamos Scientific Laboratory Report **LA-2827** (1963).
[4] W. W. Wood, J. Chem. Phys. **52**, 729 (1970).
[5] J. Vieillard-Baron, J. Chem. Phys. **56**, 4729 (1972).
[6] J. A. Cuesta and D. Frenkel, Phys. Rev. A **42**, 2126 (1990).
[7] D. Frenkel, B. M. Mulder, and J. P. McTague, Phys. Rev. Lett. **52**, 287 (1984).
[8] B. Evans, Molec. Phys. **100**, 199 (2002).
[9] D. Frenkel and B. M. Mulder, Molec. Phys. **55**, 1171 (1985).
[10] B. Mulder and D. Frenkel, Molec. Phys. **55**, 1193 (1985).
[11] M. J. Freiser, Phys. Rev. Lett. **24**, 1041 (1970).
[12] L. A. Madsen, T. J. Dingemans, M. Nakata, and E. T. Samulski, Phys. Rev. Lett. **92**, 145505 (2004).
[13] B. R. Acharya, A. Primak, and S. Kumar, Phys. Rev. Lett. **92**, 145506 (2004).
[14] J. W. Perram and E. Praestgaard, Molec. Phys. **63**, 1103 (1988).
[15] C. McBride and C. Vega, J. Chem. Phys. **117**, 10370 (2002).
[16] G.-W. Wu and R. J. Sadus, Fluid Phase Equilib. **194**, 227 (2002).
[17] M. Murat and Y. Kantor, Phys. Rev. E **74**, 031124 (2006).
[18] C. D. Michele, A. Scala, R. Schilling, and F. Sciortino, J. Chem. Phys. **124**, 104509 (2006).
[19] A. Donev, I. Cisse, D. Sachs, E. A. Variano, F. H. Stillinger, R. Connelly, S. Torquato, and P. M. Chaikin, Science **303**, 990 (2004).
[20] A. Donev, F. H. Stillinger, P. M. Chaikin, and S. Torquato, Phys. Rev. Lett. **92**, 255506 (2004).
[21] A. Donev, S. Torquato, and F. H. Stillinger, J. Comput. Phys. **202**, 737 (2005).
[22] A. Doneva, S. Torquatoa, and F. H. Stillinger, J. Comput. Phys. **202**, 765 (2005).
[23] M. G. Basavaraj, G. G. Fuller, J. Fransaer, and J. Vermant, Langmuir **22**, 6605 (2006).
[24] W. Man, A. Donev, F. H. Stillinger, M. T. Sullivan, W. B. Russel, D. Heeger, S. Inati, S. Torquato, and P. M. Chaikin, Phys. Rev. Lett. **94**, 198001 (2005).
[25] M. P. Allen, Liq. Cryst. **8**, 499 (1990).
[26] P. J. Camp and M. P. Allen, J. Chem. Phys. **106**, 6681 (1997).
[27] W. Wang, J. Wang, and M.-S. Kim, Computer Aided Geometric Design **18**, 531 (2001).
[28] J. W. Perram and M. S. Wertheim, J. Comput. Phys. **58**, 409 (1985).
[29] J. P. Straley, Phys. Rev. A **10**, 1881 (1974).
[30] R. Eppenga and D. Frenkel, Molec. Phys. **52**, 1303 (1984).
[31] C. Zannoni, in *The Molecular physics of liquid crystals*, edited by G. R. Luckhurst and G. W. Gray (Academic Press, 1979), chap. 3, p. 51.
[32] T. Boublik and I. Nezbeda, Coll. Czech. Chem. Commun. **51**, 2301 (1986).
[33] A. Isihara, J. Chem. Phys. **18**, 1446 (1950).
[34] A. Isihara and T. Hayashida, J. Phys. Soc. Jpn. **6**, 40 (1951).
[35] A. Isihara and T. Hayashida, J. Phys. Soc. Jpn. **6**, 46 (1951).
[36] I. Nezbeda, Chem. Phys. Lett. **41**, 55 (1976).
[37] J. D. Parsons, Phys. Rev. A **19**, 1225 (1979).
[38] Y. Song and E. A. Mason, Phys. Rev. A **41**, 3121 (1990).
[39] M. Rigby, Molec. Phys. **66**, 1261 (1989).
[40] M. S. Wertheim, Molec. Phys. **99**, 187 (2001).
[41] M. Maeso and J. Solana, Molec. Phys. **79**, 1365 (1993).
[42] C. Vega, Molec. Phys. **92**, 651 (1997).
[43] L. Onsager, Ann. (N.Y.) Acad. Sci. **51**, 627 (1949).
[44] A. Isihara, J. Chem. Phys. **19**, 1142 (1951).
[45] G. Zarragoicochea, D. Levesque, and J. Weis, Molec. Phys. **75**, 989 (1992).
[46] M. P. Allen and C. P. Mason, Molec. Phys. **86**, 467 (1995).
[47] C. Vega, C. McBride, and L. G. MacDowell, J. Chem. Phys. **115**, 4203 (2001).
[48] A. Samborski, G. T. Evans, C. P. Mason, and M. Allen, Molec. Phys. **81**, 263 (1994).
[49] B. Tjipto-Margo and G. T. Evans, J. Chem. Phys. **94**, 4546 (1991).
[50] W. M. Gelbart and B. Barboy, Accounts of Chemical Research **13**, 290 (1980).
[51] A. M. Somoza and P. Tarazona, Molec. Phys. **75**, 17 (1992).
[52] B. Mulder, Phys. Rev. A **39**, 360 (1989).
[53] G. S. Singh and B. Kumar, J. Chem. Phys. **105**, 2429 (1996).
[54] G. S. Singh and B. Kumar, Annals of Physics **294**, 24 (2001).